CHEMISTRY
A European Journal

A Journal of
ChemPubSoc Europe

Accepted Article

Title: Iridium(III) Complex-based Activatable Probe for Phosphorescent/Time-gated Luminescent Sensing and Imaging of Cysteine in Mitochondria of Live Cells and Animals

Authors: Zhongbo Du, Run Zhang, Bo Song, Wenzhu Zhang, Yong-Lei Wang, Jianping Liu, Chaolong Liu, Zhi Ping Xu, and Jingli Yuan

To be cited as: *Chem. Eur. J.* 10.1002/chem.201805079

Link to VoR: http://dx.doi.org/10.1002/chem.201805079

Supported by
ACES

WILEY-VCH

10.1002/chem.201805079

WILEY-VCH

FULL PAPER

Iridium(III) Complex-based Activatable Probe for Phosphorescent/Time-gated Luminescent Sensing and Imaging of Cysteine in Mitochondria of Live Cells and Animals

Zhongbo Du,[a] Run Zhang,*[b] Bo Song,[a] Wenzhu Zhang,*[a] Yong-Lei Wang,[c] Jianping Liu,[b] Chaolong Liu,[a] Zhi Ping Xu,[b] and Jingli Yuan*[a]

Abstract: This study reports an activatable iridium(III) complex probe for phosphorescence/time-gated luminescence detection of cysteine (Cys) *in vitro* and *in vivo*. The probe, **[Ir(ppy)$_2$(NTY-bpy)](PF$_6$)**, is developed by incorporating a strong electron withdrawing group, nitroolefin, into a bipyridine ligand of the Ir(III) complex. The luminescence of the probe is quenched due to the intramolecular charge transfer (ICT) process, but switched on by a specific recognition reaction between the probe and Cys. **[Ir(ppy)$_2$(NTY-bpy)](PF$_6$)** shows high sensitivity and selectivity for Cys detection and good biocompatibility. The long-lived emission of **[Ir(ppy)$_2$(NTY-bpy)](PF$_6$)** allows time-gated luminescence analysis of Cys in cells and human sera. These properties make it convenient for the phosphorescence and time-gated luminescence imaging and flow cytometry analysis of Cys in live samples. The Cys images in cancer cells and inflamed macrophage cells reveal that **[Ir(ppy)$_2$(NTY-bpy)](PF$_6$)** is distributed in mitochondria after cellular internalization. Visualizations and flow cytometry analysis of mitochondrial Cys levels and Cys-mediated redox activities of live cells are achieved. Using **[Ir(ppy)$_2$(NTY-bpy)](PF$_6$)** as a probe, *in vivo* sensing and imaging of Cys in *D. magna*, zebrafish, and mice are then demonstrated.

Introduction

Advanced biomedical diagnosis heavily relies on the determination and tracking of diseases-related biomarkers *in vitro* and *in vivo*, so that the diseases can be prevented at the early stage.[1] Biothiols, including cysteine (Cys), homocysteine (Hcy) and glutathione (GSH), have long been recognized as the most important biomarkers inside the body, where the levels of biothiols are implicated in several disorders, such as inflammation, cardiovascular diseases, and even cancers.[2] Typically, biothiols play essential roles in various physiological processes of biological systems.[3] For example, Cys and Hcy are the crucial biomolecules required for cellular growth in living organisms, and GSH is the most abundant biothiol to play a key role in redox homeostasis.[4] For Cys, deficiency of this amino acid inside the body is associated with many diseases, such as slow growth, hair depigmentation, edema, lethargy, liver damage, loss of muscle and fat, skin lesions, and weakness.[5] Abnormal level of Hcy is related to the disorders including cardiovascular disease and Alzheimer's disease.[4b] Although GSH serves as an important biomolecule in maintaining the intracellular redox activities and signal transduction, alterations in its level are implicated with liver damage, HIV infection, cancer, leucocytes loss, and psoriasis.[6]

Cells are the fundamental building block of all live organisms, and cellular organelles are the essential parts of the cell's structure and function. In live cells, mitochondria are the critical mediators of redox homeostasis because of their roles in generation and dissipation of reactive oxygen/nitrogen species (ROS/RNS).[7] The mitochondrial Cys is likely to be the key harbor for oxidative and nitrosative modifications led by highly reactive ROS/RNS, and thus Cys serves as the crucial biomolecule in mitochondria to control the critical homeostasis processes such as apoptosis, oxidative phosphorylation and redox signaling.[8] Therefore, it is of great value to engineer effective bioanalytical methods for the detection of Cys, in particular for the sensing and imaging of Cys-mediated redox signaling in mitochondria of biological systems suffering the ROS/RNS stress.[9]

Among various methods reported,[10] one of the most useful approaches would be the luminescence bioassay, where the luminescent molecular probes are developed for direct detection of biomarkers in biological milieus.[11] In consideration of main advantages of their sensitivity and selectivity, several fluorescence probes have been recently developed by conjugating biothiol-responsive units to fluorophores, such as rhodamine,[12] coumarin,[13] naphthalimide,[14] BODIPY,[15] and fluorescein.[16] Through a specific sensing mechanism, such as cyclization of aldehydes,[17] Michael addition reaction,[18] cleavage of sulfonamide and sulfonate esters,[19] and cleavage of S-S bond and Se-N bond,[20] the fluorescence signal can be modulated for quantification of biothiols. Nevertheless, the probes that can discriminate Cys from other amino acids in a specific organelle

[a] Z. Du, Dr. B. Song, Dr. W. Zhang, C. Liu, Prof. J. Yuan
State Key Laboratory of Fine Chemicals, School of Chemistry,
Dalian University of Technology,
Dalian 116024, China
E-mail: wzhzhang@dlut.edu.cn; jlyuan@dlut.edu.cn
[b] Dr. R. Zhang, J. Liu, Prof. Z. P. Xu
Australian Institute for Bioengineering and Nanotechnology,
The University of Queensland,
St. Lucia, QLD 4072, Australia
E-mail: r.zhang@uq.edu.au
[b] Dr. Y.-L. Wang
Department of Chemistry,
Stanford University,
Stanford, California 94305, United States

Supporting information for this article is given via a link at the end of the document. General information for experiments, synthesis and characterisation of probe, theoretical computation, spectrometric response, supplementary figures and schemes, and cell imaging and flow cytometry analysis.

10.1002/chem.201805079

are scarcely reported.[21] In this context, development of responsive phosphorescence probes for sensing and imaging of Cys at subcellular levels, in particular for detection of Cys-mediated redox activities in mitochondria, is urgently demanded.

In past several years, transition metal complex-based activatable phosphorescence probes that can be used for sensing and imaging of important biomarkers have been attracted considerable attention due to their unique photophysical, photochemical, and electrochemical properties.[22] Among these metal complexes, cyclometalated Ir(III) complexes are particularly intriguing due to their several favorable photophysical properties for luminescence bioassays:[23] i) tunable luminescence emissions with variations of coordinative ligands; ii) high stability under ambient conditions and bright luminescence emissions; iii) large Stokes shift; iv) resistance to photobleaching; v) low cytotoxicity; vi) long emission lifetime; and vii) cell organelle-targetable feature.[24] In previous researches, we have also confirmed the capability of Ir(III) complex-based responsive phosphorescence probes for the detection of biomarkers, such as reactive oxygen species,[25] and methylglyoxal *in vitro* and *in vivo*.[26] These facts promote us to design a unique Ir(III) complex phosphorescence probe for highly sensitive detection of Cys, and for further studies of Cys-mediated redox activities in biological systems.

In this contribution, a functional Ir(III)-phenylpyridine complex derivative **[Ir(ppy)$_2$(NTY-bpy)](PF$_6$)** [ppy: 2-phenylpyridine; NTY-bpy: 4-methyl-4'-(2-nitrovinyl)-2,2'-bipyridine], is reported for the sensing and imaging of Cys *in vitro* and *in vivo* (**Scheme 1**). Due to a strong electron withdrawing group coupled to the 2,2'-bipyridine ligand, the phosphorescence emission of **[Ir(ppy)$_2$(NTY-bpy)](PF$_6$)** is quenched by intramolecular charge transfer (ICT) process. In the presence of Cys, a specific recognition reaction between the complex and Cys occurs, which affords the product, **[Ir(ppy)$_2$(Cys-bpy)](PF$_6$)**. With this specific reaction, remarkable "OFF-ON" phosphorescence response could be obtained for Cys detection. The recognition reaction between **[Ir(ppy)$_2$(Cys-bpy)](PF$_6$)** and Cys was confirmed by HRMS analysis and Griess test. The "OFF-ON" phosphorescence response was rationalized by DFT/TD-DFT computations. The data of spectrometric titration analysis reveals that **[Ir(ppy)$_2$(NTY-bpy)](PF$_6$)** can sensitively respond to Cys over other amino acids. **[Ir(ppy)$_2$(NTY-bpy)](PF$_6$)** features low cytotoxicity and cell membrane permeability, which enables it suitable as a probe for detection of Cys in living biological samples. **[Ir(ppy)$_2$(NTY-bpy)](PF$_6$)** and **[Ir(ppy)$_2$(Cys-bpy)](PF$_6$)** exhibited long emission lifetimes, facilitating the time-gated luminescence analysis of Cys in human sera and visualization of Cys in live cells.[27] Luminescent imaging and flow cytometry analysis of Cys in mitochondria of live cells as well as luminescent imaging of Cys in *D. magna*, zebrafish, and mouse were then performed. In particular, the visualization of Cys-mediated redox in inflammatory mimic macrophage cells was achieved, which suggests that **[Ir(ppy)$_2$(NTY-bpy)](PF$_6$)** could be a promising probe for further biomedical applications in early diagnosis and treatment monitoring of inflammation diseases.

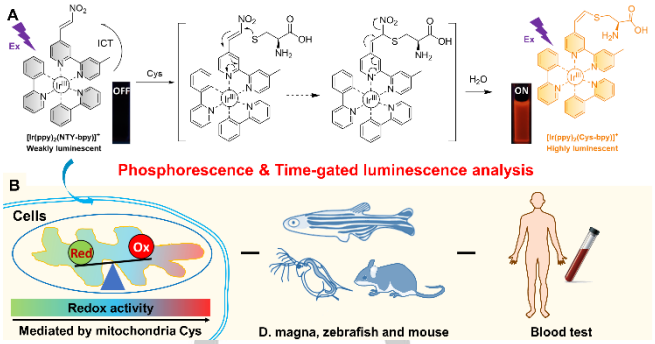

Scheme 1. Schematic illustration of the luminescence response mechanism of **[Ir(ppy)$_2$(NTY-bpy)](PF$_6$)** towards Cys (A) and the application of **[Ir(ppy)$_2$(NTY-bpy)](PF$_6$)** for phosphorescence and time-gated luminescence analysis of Cys-mediated mitochondria redox activity, Cys in *D. magna*, zebrafishand mouse, and Cys in human blood sera.

Results and Discussion

Design, synthesis and characterization of the iridium(III) complex probe

Transition metal complex-based luminescent probes have provided an alternative approach for the analysis of biomolecules *in vitro* and *in vivo*.[22i, 28] Among phosphorescence probes, phosphorescent Ir(III) complexes contribute significantly to the development of activatable probes for bioassay and bioimaging due to their abundant photochemical, photophysical, and electrochemical properties.[29] Considering the important roles of Cys in biological systems and the unique properties of Ir(III) complexes, we developed Ir(III) complex-based responsive probes for phosphorescence and time-gated luminescence detection of Cys in aqueous and live organisms.

An Ir(III) complex-based probe, **[Ir(ppy)$_2$(NTY-bpy)]$^+$**, was designed by coupling a nitroolefin moiety to the bipyridine ligand for specifically responding to Cys. In the presence of Cys, this nitroolefin moiety can react with the mercapto group of Cys through a 1,4-addition reaction,[30] followed by the removal of nitro group to form the product **[Ir(ppy)$_2$(Cys-bpy)]$^+$** (**Scheme 1**). Due to the incorporation of strong electron withdrawing nitroolefin moiety into the Ir(III) complex, the emission of **[Ir(ppy)$_2$(NTY-bpy)]$^+$** is expected to be quenched by the ICT process. While the luminescence can be switched-on by the corruption of ICT process after removal of nitro group. More importantly, considering the intrinsic cationic lipophilicity of the Ir(III) complex, **[Ir(ppy)$_2$(NTY-bpy)]$^+$** is anticipated to be accumulated in mitochondria after cellular uptake, thereby the subcellular concentration level of Cys can be visualized.

The NTY-bpy ligand was firstly synthesized by the reaction of CHO-bpy with nitromethane in anhydrous toluene (Scheme S1, Supporting Information). This ligand was then subjected to a coordination reaction with [Ir$_2$(ppy)$_4$Cl$_2$] in MeOH-CH$_2$Cl$_2$ to yield the corresponding Ir(III) complex, **[Ir(ppy)$_2$(NTY-bpy)](PF$_6$)**. The chemical structure of the ligand NTY-bpy and **[Ir(ppy)$_2$(NTY-bpy)](PF$_6$)** was confirmed by NMR, ESI-MS, HRMS, and elemental analysis (Figures S1-S5, Supporting Information).

The product of **[Ir(ppy)$_2$(NTY-bpy)]$^+$** reacting with Cys was further investigated by ESI-MS analysis. Upon addition of Cys into **[Ir(ppy)$_2$(NTY-bpy)]$^+$** solution, the peak at *m/z* = 816.25 was observed, which can be assigned to **[Ir(ppy)$_2$(Cys-bpy)]$^+$** (Figure S6, Supporting Information). The result of HRMS showed the peak at *m/z* = 816.1969 (Figure S7, Supporting Information), which can also be ascribed to **[Ir(ppy)$_2$(Cys-bpy)]$^+$** (calcd. *m/z* = 816.1961). To confirm the removal of the nitrite ion, Griess reagent was added to the reaction solution of **[Ir(ppy)$_2$(NTY-bpy)]$^+$** and Cys, and the UV-vis spectra were measured. The absorption spectra of **[Ir(ppy)$_2$(NTY-bpy)]$^+$** and Griess reagent were measured as the controls. Intense absorption band at 450-600 nm was observed, indicating the release of nitrite after the reaction (Figure S8, Supporting Information).

Photophysical properties of the iridium(III) complex probe

The photophysical properties of **[Ir(ppy)$_2$(NTY-bpy)]$^+$** and its reaction product with Cys, **[Ir(ppy)$_2$(Cys-bpy)]$^+$**, were then investigated. In the absence and presence of Cys, UV-vis absorption spectra of **[Ir(ppy)$_2$(NTY-bpy)]$^+$** were firstly measured. As shown in **Figure 1**A, for all the UV-vis spectra, the strong absorption bands at around 280-320 nm could be assigned to the spin-allowed intraligand charge transitions (^{1}ILCT) of ligands ppy and NTY-bpy. Moderate intense absorption bands in the visible region were also observed, which can be ascribed to the overlap of the spin-allowed metal-to-ligand charge transfer (^{1}MLCT), ligand-to-ligand charge transfer (^{1}LLCT), and the ^{1}ILCT. In the presence of Cys, decrease of the absorption band centered at 380 nm was noticed, which might be caused by the corruption of ^{1}ILCT transition after the reaction of **[Ir(ppy)$_2$(NTY-bpy)]$^+$** with Cys.

As shown in **Figure 1**B, under excitation at 380 nm, **[Ir(ppy)$_2$(NTY-bpy)]$^+$** displayed very weak phosphorescence, ascribed to the effective quenching induced by ICT from Ir(III) center to nitroolefin moiety. As expected, intense phosphorescence at 590 nm was emitted after the reaction of **[Ir(ppy)$_2$(NTY-bpy)]$^+$** with Cys. This result indicates that the phosphorescence of **[Ir(ppy)$_2$(NTY-bpy)]$^+$** can be switched-on in the presence of Cys owing to the production of **[Ir(ppy)$_2$(Cys-bpy)]$^+$** (quantum yield, ϕ = 4.36%, Table S1, Supporting Information).

Both **[Ir(ppy)$_2$(NTY-bpy)](PF$_6$)** and **[Ir(ppy)$_2$(Cys-bpy)](PF$_6$)** feature a large Stokes shift (> 200 nm), with absorption peaks at 380 nm and emission peaks at 600 nm and 590 nm, respectively. The emission lifetime of **[Ir(ppy)$_2$(NTY-bpy)](PF$_6$)** and **[Ir(ppy)$_2$(Cys-bpy)](PF$_6$)** were determined to be 86 ns (Figure S9, Supporting Information) and 103 ns (Figure S10, Supporting Information), respectively. The long emission lifetime enables the assay of Cys to be performed in a background free time-gated luminescence mode.

Theoretical calculation

To deepen the discussion about the electronic structure, electron transfer, and photophysical properties of **[Ir(ppy)$_2$(NTY-bpy)]$^+$** before and after reaction with Cys, specific investigations on the theoretical level, *i. e.,* density functional theory (DFT) and time-dependent DFT (TD-DFT) computations, were performed to evaluate the corresponding transition energies of **[Ir(ppy)$_2$(NTY-bpy)]$^+$** and **[Ir(ppy)$_2$(Cys-bpy)]$^+$**. The ground-state (S_0) and excited state (T_1) geometries of **[Ir(ppy)$_2$(NTY-bpy)]$^+$** and **[Ir(ppy)$_2$(Cys-bpy)]$^+$** were optimized taking into account effects of bulk solvent (H_2O) by means of the polarizable continuum model (PCM). By DFT calculation, the molecular geometries of **[Ir(ppy)$_2$(NTY-bpy)]$^+$** and **[Ir(ppy)$_2$(Cys-bpy)]$^+$** were obtained as displayed in Figures S11, S12 (Supporting Information). The corresponding optimized geometrical parameters in S_0 and T_1 states are shown in Table S2, S3 (Supporting Information).

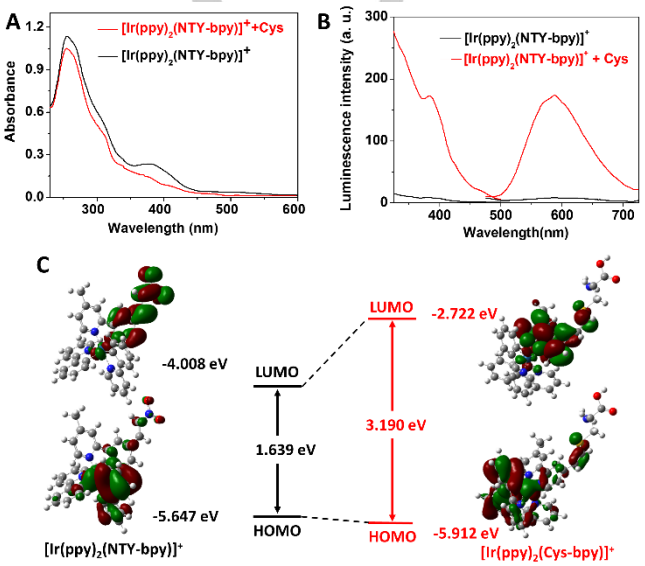

Figure 1. (A) UV-vis absorption spectra of **[Ir(ppy)$_2$(NTY-bpy)]$^+$** (20 μM) and (B) phosphorescence spectra of **[Ir(ppy)$_2$(NTY-bpy)]$^+$** (10 μM) in the absence and presence of Cys (20 μM). λ_{ex} = 380 nm, λ_{em} = 590 nm. (C) Frontier molecular orbital distributions (HOMO and LUMO) of **[Ir(ppy)$_2$(NTY-bpy)]$^+$** and **[Ir(ppy)$_2$(Cys-bpy)]$^+$** at their optimized geometries of lowest triplet excited states (T_1). The energy levels of the MOs are shown.

Optimized molecular geometries clearly exhibit the π-conjugation extended to C=C double bond for both **[Ir(ppy)$_2$(NTY-bpy)]$^+$** (Figure S11, Supporting Information) and **[Ir(ppy)$_2$(Cys-bpy)]$^+$** (Figure S12, Supporting Information). Based on the optimized ground state molecular geometries, the highest occupied molecular orbital (HOMO), lowest unoccupied molecular orbital (LUMO), and nearby molecular orbitals were calculated (Figures S13, S14, Supporting Information). For **[Ir(ppy)$_2$(NTY-bpy)]$^+$**, orbital analyses show that the HOMOs are mainly located on the Ir(III) centre and ppy ligands, with small distribution on the 4-methylpyridine of NTY-bpy ligand in HOMO-2. LUMOs of **[Ir(ppy)$_2$(NTY-bpy)]$^+$** are distributed on the NTY-bpy ligand. Interestingly, LUMO of **[Ir(ppy)$_2$(NTY-bpy)]$^+$** clearly shows major contribution from the 4-(2-nitrovinyl)pyridine, rather than the whole bipyridine moiety.

Based on the optimized ground state molecular geometries of **[Ir(ppy)$_2$(NTY-bpy)]$^+$** and **[Ir(ppy)$_2$(Cys-bpy)]$^+$**, TD-DFT calculations were carried out to explore the electronic transitions

corresponding to their absorption profiles. As shown in Table S4 (Supporting Information), the electronic transition from the ground state to the first excited singlet state (S_1) is mainly contributed by HOMO→LUMO, which could be assigned to ^{1}MLCT and ^{1}LL'CT characters (L: ppy; L': NTY-bpy or Cys-bpy). These ^{1}MLCT, ^{1}LL'CT, and ^{1}L'LCT transitions were noticed in all excited singlet states (S_1-S_7) of both **[Ir(ppy)$_2$(NTY-bpy)]$^+$** and **[Ir(ppy)$_2$(Cys-bpy)]$^+$**.

To further examine the phosphorescence "OFF-ON" response, TD-DFT calculations were performed to understand the emission electronic transitions at the lowest-lying triplet excited state optimized molecular geometries of **[Ir(ppy)$_2$(NTY-bpy)]$^+$** and **[Ir(ppy)$_2$(Cys-bpy)]$^+$**. The emission electronic transitions (T_1-T_8) of **[Ir(ppy)$_2$(NTY-bpy)]$^+$** and **[Ir(ppy)$_2$(Cys-bpy)]$^+$**) are exhibited in Table S5 (Supporting Information), and the representative frontier molecular orbital distributions of **[Ir(ppy)$_2$(NTY-bpy)]$^+$** and **[Ir(ppy)$_2$(Cys-bpy)]$^+$** are presented in Figures S15, S16 (Supporting Information). The molecular orbital distributions of **[Ir(ppy)$_2$(NTY-bpy)]$^+$** and **[Ir(ppy)$_2$(Cys-bpy)]$^+$** in triplet states were noticed to be similar to that of molecular orbital distributions in S_0 states. In **[Ir(ppy)$_2$(NTY-bpy)]$^+$**, ^{1}T is mainly involved (95.8%) in the HOMO→LUMO transition (Table S5, Supporting Information). As shown in **Figure 1**C, this transition can be attributed to the ^{3}MLCT and ^{3}LL'CT characters. Charge transfer to NTY moiety was clearly noticed from the HOMO→LUMO transition of **[Ir(ppy)$_2$(NTY-bpy)]$^+$**. As the result, the luminescence of **[Ir(ppy)$_2$(NTY-bpy)]$^+$** is quenched. In **[Ir(ppy)$_2$(Cys-bpy)]$^+$**, T_1 is mainly contributed by the transition from HOMO→LUMO (57.1%) with small contribution from HOMO-2→LUMO (13.1%) and HOMO-1→LUMO (12.3%) transitions. These transitions exhibit obvious ^{3}MLCT and ^{3}LL'CT characters. The emissive transitions, including ^{3}MLCT, ^{3}L'LCT and ^{3}L'LCT of T_1 and other triplet excited states, are consistent with the typical photophysical properties of iridium(III) complexes. Therefore, the phosphorescence emission is switched-on when **[Ir(ppy)$_2$(NTY-bpy)]$^+$** is transferred to **[Ir(ppy)$_2$(Cys-bpy)]$^+$** in the presence of Cys.

Phosphorescence turn-on response of [Ir(ppy)$_2$(NTY-bpy)](PF$_6$) to Cys

Emission spectrum response of **[Ir(ppy)$_2$(NTY-bpy)]$^+$** towards different concentrations of Cys was firstly investigated after incubation of **[Ir(ppy)$_2$(NTY-bpy)]$^+$** and Cys for 30 min. As shown in **Figure 2**A, the emission intensity was gradually increased with increasing the Cys concentration. The dose-dependent emission enhancement exhibited a good linearity in the concentration range of 0-10.0 μM (Figure S17, Supporting Information). The detection limit was calculated to be 86 nM based on the reported methods defined by IUPAC. These data indicate that **[Ir(ppy)$_2$(NTY-bpy)]$^+$** can be used for highly sensitive phosphorescence detection of Cys.

To confirm the phosphorescence response specificity of the probe to Cys, the phosphorescence intensity of **[Ir(ppy)$_2$(NTY-bpy)]$^+$** after reaction with various amino acids was recorded. As shown in **Figure 2**B, upon reaction with 10 μM of Cys, the phosphorescence intensity was remarkably increased, while negligible luminescence increases were noticed even though **[Ir(ppy)$_2$(NTY-bpy)]$^+$** was reacted with 500 μM of other amino acids. These results demonstrate high specificity of the phosphorescence response of **[Ir(ppy)$_2$(NTY-bpy)]$^+$** towards Cys.

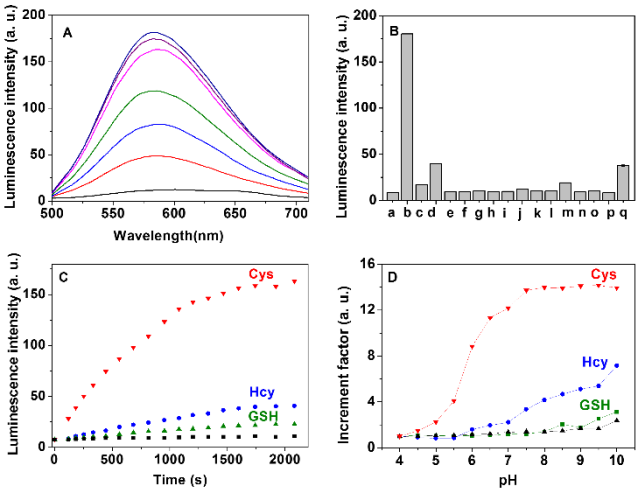

Figure 2. (A) Emission spectra of **[Ir(ppy)$_2$(NTY-bpy)]$^+$** (10 μM) reacted with different concentrations of Cys (0-10 μM). (B) Phosphorescence intensities of **[Ir(ppy)$_2$(NTY-bpy)]$^+$** (10 μM) reacted with various amino acids. (a) Blank, (b) Cys, (c) GSH, (d) Hcy, (e) Trp, (f) Thr, (g) Gly, (h) Val, (i) Leu, (j) His, (k) Pro, (l) Ser, (m) Tyr, (n) Ala, (o) Asp, (p) Arg, ,(q) human serum albumin (HSA, 100 μM). (C) Time-profile phosphorescence response and (D) pH effect on the phosphorescence response of **[Ir(ppy)$_2$(NTY-bpy)]$^+$** (10 μM) (black line) towards biothiols (10 μM for Cys, red line; 20 μM for Hcy, blue line; and 20 μM for GSH, green line) in CH_3CN-PBS buffer (25 mM, pH 7.4, 1/1, v/v). λ_{ex}= 380 nm, λ_{em}= 590 nm.

As the similar chemical structure of Cys, Hcy, and GSH, small enhancement in phosphorescnece intensity was also noticed upon the addition of Hcy and GSH (10 μM). To confirm the selectivity of **[Ir(ppy)$_2$(NTY-bpy)]$^+$** towards Cys over other biothiols, time-dependent phosphorescence responses of **[Ir(ppy)$_2$(NTY-bpy)]$^+$** towards Cys, Hcy and GSH were investigated by recording the changes of the emission intensity at 590 nm. As shown in **Figure 2**C, **[Ir(ppy)$_2$(NTY-bpy)]$^+$** solution exhibited weak and stable emission under continuous excitation at 380 nm. After adding Cys, the phosphorescence intensity was gradually increased, and reached a maximum value at ~30 min, indicating that the reaction between **[Ir(ppy)$_2$(NTY-bpy)]$^+$** and Cys was completed within 0.5 h. For Hcy and GSH, slight enhancement in the luminescence intensity was observed after incubation for up to 2 h (Figure S18, Supporting Information), which indicates that **[Ir(ppy)$_2$(NTY-bpy)]$^+$** has the potential to distinguish Cys from Hcy and GSH.

The effects of pH on the phosphorescence responses of **[Ir(ppy)$_2$(NTY-bpy)]$^+$** towards Cys, Hcy and GSH were further examined by recording the phosphorescence intensity changes at 590 nm in the absence and presence of three biothiols. As shown in **Figure 2**D, the phosphorescence intensity of **[Ir(ppy)$_2$(NTY-bpy)]$^+$** was found to be weak and stable in PBS buffers with different pH values ranged from 4.0 to 10.0. Upon reaction with

Cys, the phosphorescence intensity was gradually increased in the range of pH 4.5-7.5, and the maximum phosphorescence intensity was obtained at pH 7.5. In contrast, no obvious phosphorescence enhancement was observed after probe solution reacted with GSH. Increasing pH (>7) enhanced the phosphorescence intensity of **[Ir(ppy)$_2$(NTY-bpy)]$^+$**-Hcy solution slightly. Phosphorescence response of **[Ir(ppy)$_2$(NTY-bpy)]$^+$** towards Hcy in alkaline solution could be attributed to the higher pKa value of Hcy (pKa = 10.0).[31] Together with the slow responses of **[Ir(ppy)$_2$(NTY-bpy)]$^+$** towards Hcy and GSH (**Figure 2**C), the high reactivity of **[Ir(ppy)$_2$(NTY-bpy)]$^+$** with Cys may be attributed to the high nucleophilicity of its -SH group in biological pH level (pKa of Cys is 8.53, compared with 10.0 of Hcy and 9.20 of GSH) and its weak steric effect.[21b, 31]

Time-gated luminescence analysis of Cys

Thanks to the long emission lifetime of **[Ir(ppy)$_2$(NTY-bpy)]$^+$** and **[Ir(ppy)$_2$(Cys-bpy)]$^+$**, time-gated luminescence analysis of Cys was performed in PBS buffer using LysoSensor^{TM} Green (30 μM) as the artificial background interference. As shown in Figure S19A (Supporting Information), only fast emission decay process of LysoSensor^{TM} Green was noticed without Cys added. By contrast, both fast and slow emission decay processes were observed after the addition of Cys (Figure S19C, Supporting Information). This slow emission decay can be attributed to the long-lived emission of **[Ir(ppy)$_2$(Cys-bpy)]$^+$**. With the excitation at 405 nm, this probe solution exhibited intense green emission, and such an emission spectrum was not changed in the presence of Cys (Figure S19B, Supporting Information). However, the background green emission was effectively removed by time-gated analysis with a 50 ns delay. Significant enhancement in luminescence at 590 nm was observed after reaction with Cys (Figure S19D, Supporting Information). These data suggests the potential of [Ir(ppy)$_2$(NTY-bpy)]$^+$ for the background-free time-gated luminescence detection of Cys.

Thus, time-gated luminescence response of **[Ir(ppy)$_2$(NTY-bpy)]$^+$** towards different concentrations of Cys was examined by the titration. As shown in **Figure 3**A, time-gated luminescence intensity of **[Ir(ppy)$_2$(NTY-bpy)]$^+$** was gradually increased after reaction with the increasing Cys concentration, and the intensity showed a good linearity with the Cys concentration in the range of 0-10 μM (**Figure 3**B), which indicates that the Cys level can be quantified by time-gated luminescence analysis.

On the basis of these data, the concentration level of Cys in human sera was determined with the time-gated luminescence method. The sera were collected from healthy volunteers, and then 100-fold diluted with PBS buffer before the addition of **[Ir(ppy)$_2$(NTY-bpy)]$^+$**. As shown in **Figure 3**C, weak autofluorescence from serum samples was noticed even after 100-fold dilution, while such a background signal was effectively removed using time-gated mode (**Figure 3**D). Upon mixing with 100-times diluted human sera for 0.5 h, phosphorescence and time-gated luminescence was 6.4-fold and 9.1-fold enhanced, respectively. Further enhancements in both phosphorescence and time-gated luminescence were observed in the presence of Cys. Using the standard curve shown in **Figure 3**B, the concentration of Cys in human sera was determined to be 254 ± 16 μM, which is consistent with the reported.[15d] By adding exogenous Cys into the diluted human sera, the recovery of added Cys was determined to be 89.8-90.5% (Table S6, Supporting Information), indicating that the time-gated luminescence analysis of Cys using **[Ir(ppy)$_2$(NTY-bpy)]$^+$** as a probe is highly accurate.

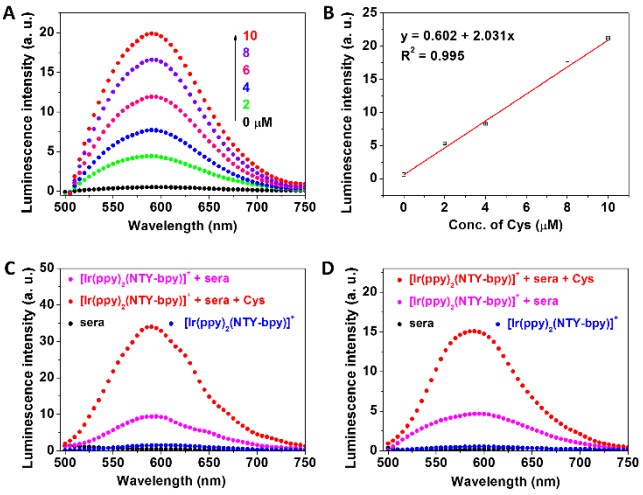

Figure 3. (A) Time-gated luminescence spectra of **[Ir(ppy)$_2$(NTY-bpy)]$^+$** (10 μM) in the presence of different concentration of Cys; (B) standard curve for the time-gated luminescence detection of Cys; (C) phosphorescence and (D) time-gated luminescence analysis of Cys in human serum samples with **[Ir(ppy)$_2$(NTY-bpy)]$^+$** (10 μM) as a probe (exogenous Cys addition: 5 μM)..

Imaging of Cys in live cells

Prior to the imaging application, the cytotoxicity of **[Ir(ppy)$_2$(NTY-bpy)]$^+$** towards MCF-7 cells and J774A.1 macrophage cells was evaluated by MTT assay and PrestoBule^{TM} viability assay, respectively. Upon incubating MCF-7 cells with **[Ir(ppy)$_2$(NTY-bpy)]$^+$** at the concentrations of 0, 10, 20, 40, 100, and 200 μM, remarkable effects on the cell proliferation were not observed (Figure S20, Supporting Information). The cell viability remained at over 67% even after co-incubating MCF-7 cells with 200 μM **[Ir(ppy)$_2$(NTY-bpy)]$^+$** for 24 h. Then, the cytotoxicity of **[Ir(ppy)$_2$(NTY-bpy)]$^+$** towards J774A.1 macrophage cells was assessed by PrestoBlue^{TM} cell viability assay. The data showed that the cell viability remained to be about 84% after J774A.1 cells were incubation with 200 μM of **[Ir(ppy)$_2$(NTY-bpy)]$^+$** for 24 h. The results indicate that the cytotoxicity of **[Ir(ppy)$_2$(NTY-bpy)]$^+$** is very limited. Because a very low concentration of the complex (10-30 μM) is normally used for the cell imaging, the cytotoxicity at these concentrations is negligible.

To determine the time profile of the intracellular luminescence intensity, MCF-7 cells were incubated with 10 μM **[Ir(ppy)$_2$(NTY-bpy)]$^+$** for different times (0.5, 1, 2, 3, 5 h), and then the MFI was measured by flow cytometry. As shown in Figure S21 (Supporting Information), significant enhancement of MFI was observed for MCF-7 cells incubated with **[Ir(ppy)$_2$(NTY-bpy)]$^+$** within 2 h. After

10.1002/chem.201805079

2 h, increase of mean luminescence intensity (MFI) became rather slow. This result suggests that the imaging of Cys in live cells could be performed within 1-2 h co-incubation.

As shown in Figure S22 (Supporting Information), clear red luminescence was observed after MCF-7 cells were incubated with 10 μM of **[Ir(ppy)$_2$(NTY-bpy)]$^+$** for 2 h. To confirm the intracellular luminescence was indeed originated from the reaction product of **[Ir(ppy)$_2$(NTY-bpy)]$^+$** with Cys, MCF-7 cells were pretreated with 500 μM NEM (N-ethylmaleimide) for 1 h, followed by the incubation with **[Ir(ppy)$_2$(NTY-bpy)]$^+$** for 2 h. In this case, the cells showed weak luminescence as the biothiols were scavenged by NEM (Figure S22B, Supporting Information). In another group, after NEM treatment and **[Ir(ppy)$_2$(NTY-bpy)]$^+$** incubation, the cells were supplied with 200 μM of Cys for another 1 h. Significant luminescence was observed again (Figure S22C, Supporting Information). To quantify the changes of intracellular luminescence in different conditions, flow cytometry analysis was performed to record the luminescence intensity of each cell population of MCF-7 cells. The MFI of the **[Ir(ppy)$_2$(NTY-bpy)]$^+$**-loaded cells was significantly decreased when the intracellular Cys was scavenged by NEM, while the further incubation with Cys recovered the intracellular luminescence intensity (Figure S23, Supporting Information).

The intracellular images also shows that the red luminescence signals were not even in the cytoplasm. This observation implies the subcellular localization of the luminescent products of **[Ir(ppy)$_2$(NTY-bpy)]$^+$** reacted with Cys in MCF-7 cells. Considering the character of mitochondria accumulation of cationic Ir(III) complexes,[32] the **[Ir(ppy)$_2$(NTY-bpy)]$^+$**-loaded MCF-7 cells were then incubated with MitoTracker™ Green FM to confirm its mitochondria distribution after cellular uptake. Clear yellow luminescence (overlap of red luminescence from the product of **[Ir(ppy)$_2$(NTY-bpy)]$^+$** reacted with Cys and green fluorescence from MitoTracker™ Green FM) in MCF-7 cells was observed (Figure S24, Supporting Information). The intensity profile of linear regions of interests across MCF-7 cells (ROIs 1 and 2) shows obviously synchronous luminescence signals, suggesting the co-localization of **[Ir(ppy)$_2$(NTY-bpy)]$^+$** and MitoTracker™ Green FM in MCF-7 cells. The Pearson's correlation coefficients and the Mander's overlap coefficients were determined to be 0.852 and 0.867, respectively. Both coefficients are close to 1 in the colocalization analysis, indicating that the majority of **[Ir(ppy)$_2$(NTY-bpy)]$^+$** localized within mitochondria of MCF-7 cells. This localization feature shows that the Cys levels in mitochondria of live cells can be visualized by using **[Ir(ppy)$_2$(NTY-bpy)]$^+$** as a probe.

Considering the importance of photostability of the luminescence probes for optical analysis and imaging, the resistance to photobleaching of **[Ir(ppy)$_2$(NTY-bpy)]$^+$** and **[Ir(ppy)$_2$(Cys-bpy)]$^+$** was examined in buffer solution and live cells. As shown in Figure S25 (Supporting Information), no obvious changes of the phosphorescence intensity were noticed for **[Ir(ppy)$_2$(NTY-bpy)]$^+$** and **[Ir(ppy)$_2$(Cys-bpy)]$^+$** solutions after UV irradiation for 2 h. The stability was then confirmed by imaging, where the cell images were recorded for 10 times at 100% laser power. As shown in Figure S26 (Supporting Information), no changes of intracellular signals were observed after scanning for 10 times, indicating the high stability of the Ir(III) complexes to resist the photobleaching.

Using **[Ir(ppy)$_2$(NTY-bpy)]$^+$** as a probe, we then demonstrated the time-gated luminescence imaging of Cys in live MCF-7 cells. MCF-7 cells were incubated with **[Ir(ppy)$_2$(NTY-bpy)]$^+$**, followed by staining with LysoSensor™ Green (the artificial noise signal) and Hoechst 33342 (staining for nuclei). As shown in **Figure 4**A-D, blue channel stained with Hoechst 33342 showed consistent fluorescence without time-gating. Under pulsed laser excitation (470 nm), intense intracellular green and red emissions were observed for the signals recorded within 0-12 ns (**Figure 4**A). With time-gating at 0-6 ns (**Figure 4**B), intracellular emission intensity was decreased to 68.8 ± 10.7% (green channel) and 61.1 ± 4.6% (red channel), compared to control group shown in **Figure 4**A. While with the imaging time delayed for 6 and 8 ns, the emission of green channel decreased dramatically, to 29.9 ± 3.1% and 16.1 ± 4.2%, which is in contrast with the emission of red channel (>40%, **Figure 4**E). From 3D surface interactive intensity analysis of images shown in **Figure 4**A, B, the intensity of green channel was higher than that of red channel. However, with time delayed for 6 and 8 ns, the intracellular green emission was remarkably weakened, while the red emission was nearly the same (**Figure 4**C, D). This is consistent with the increased signal to noise (S/N) ratio (**Figure 4**F), highlighting the advantages of time-gated luminescence cell imaging.

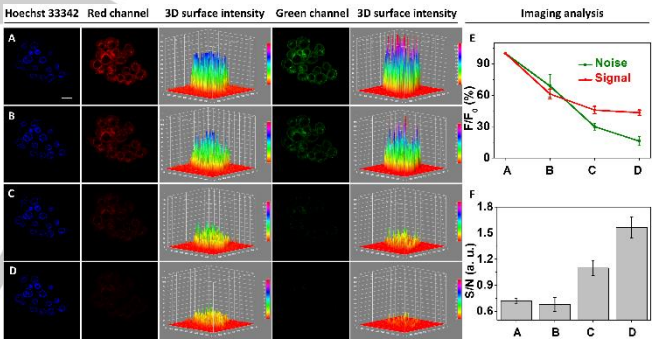

Figure 4. Time-gated luminescence imaging of Cys in MCF-7 cells. MCF-7 cells were incubated with **[Ir(ppy)$_2$(NTY-bpy)]$^+$** (10 μM) for 2 h, followed by staining with Hoechst 33342 and LysoSensor™ Green. The signal from red and green channel were collected within 0-12 ns (A); 0-6 ns (B); 6-12 ns (C); and 8-12 ns (D). (E) Changes of intracellular red and green signal of group A-D; (F) signal to noise ratio of the images of group A-D. Scale bar, 10 μm.

It is known that high levels of reactive oxygen species (ROS) can be generated during the inflammatory response of macrophage cells. In a previous research, we have demonstrated the formation of H_2S at a higher concentration level in J774A.1 inflamed macrophage cells.[45] As one of the most important antioxidants and the substrate for generating H_2S, Cys is envisaged to be decreased in its concentration during the inflammation of macrophage cells. To investigate the Cys level changes in this process, J774A.1 macrophage cells were treated with 5.0 ng/mL lipopolysaccharide (LPS) for 2 h, followed by incubation with **[Ir(ppy)$_2$(NTY-bpy)]$^+$** for another 2 h. As shown in **Figure 5**B, nearly no luminescence of live J774A.1 cells was

10.1002/chem.201805079

observed, obviously different from that in control group cells (**Figure 5**A, incubated with 10 μM **[Ir(ppy)$_2$(NTY-bpy)]$^+$** only for 2 h). Then, the cells were supplied with 200 μM of Cys for 1 h. Bright red luminescence signals from the cells were noticed (**Figure 5**C). The luminescence intensity is almost the same as that of the group where J774A.1 cells were supplied with 200 μM Cys for 1 h before staining with **[Ir(ppy)$_2$(NTY-bpy)]$^+$** (**Figure 5**D).

Similar to the distribution of **[Ir(ppy)$_2$(NTY-bpy)]$^+$** in mitochondria of MCF-7 cells, the localization of **[Ir(ppy)$_2$(NTY-bpy)]$^+$** in this organelle in live J774A.1 cells was also noticed. The images with obviously overlapped yellow luminescence were obtained for the J774A.1 cells stained with both **[Ir(ppy)$_2$(NTY-bpy)]$^+$** and MitoTracker™ Green FM (**Figure 5**E-J). The mitochondria localization was supported by the synchronous luminescence signals in the linear region of interest (ROIs 1 and 2) across the cells (**Figure 5**K-L). Both Pearson's correlation coefficients (0.895) and Mander's overlap coefficients (0.904) are close to 1, revealing that the majority of **[Ir(ppy)$_2$(NTY-bpy)]$^+$**-loaded vesicles localized within mitochondria of J774A.1 cells. The intensity correlation quotient (ICQ) for two stains was confirmed to be 0.426, which is close to 0.5, indicating that the stains of **[Ir(ppy)$_2$(NTY-bpy)]$^+$** and MitoTracker™ Green FM were dependent.

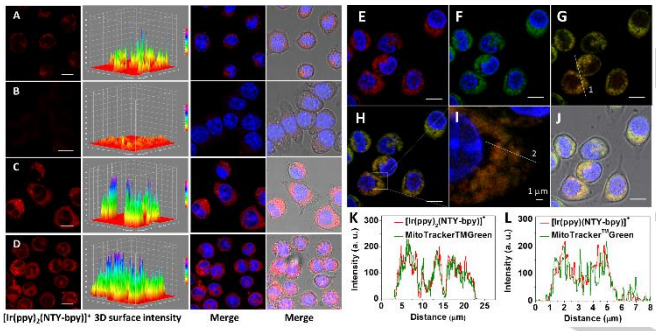

Figure 5. (A-D) Luminescence imaging and 3D surface interactive intensity analysis of Cys in inflamed J774A.1 macrophage cells. (A) J774A.1 macrophage cells were incubated with **[Ir(ppy)$_2$(NTY-bpy)]$^+$** (10 μM) for 2 h; (B) J774A.1 cells were treated with LPS (5.0 ng/mL) for 1 h, and then stained with **[Ir(ppy)$_2$(NTY-bpy)]$^+$** (10 μM) for 2 h; (C) the group B cells were further supplied with Cys (200 μM) for another 1 h; (D) J774A.1 macrophage cells were treated with Cys (200 μM) for 1 h, and then incubated with **[Ir(ppy)$_2$(NTY-bpy)]$^+$** (10 μM) for another 2 h. (E-L) Intracellular colocalization luminescence imaging of J774A.1 cells. The cells were incubated with **[Ir(ppy)$_2$(NTY-bpy)]$^+$** (10 μM) for 2 h, followed by staining with MitoTracker™ Green FM and Hoechst 33342. (E) Merged image of red and blue channels; (F) merged image of green and blue channels; (G) merged image of red and green channels; (H) merged image of red, blue and green channels; (I) the zoom-in image of the cell shown in the dashed box in H; (J) merged image of H and bright-field. (K, L) Luminescence intensity profiles of the regions of interests (ROIs) across J774A.1 macrophage cells (line 1 in G and line 2 in I). Scale bar, 10 μm.

The evolution of Cys levels in inflamed J774A.1 macrophage cells at large scale cell populations was further investigated, where the MFI was analysed by flow cytometry. As shown in Figure S27 (Supporting Information), the LPS-stimulated J774A.1 macrophage cells showed only weak luminescence, while the MFI was significantly increased after supplying the inflamed cells with Cys. The luminescence intensity was found to be similar to that of the group where J774A.1 cells were treated with Cys directly before incubation with **[Ir(ppy)$_2$(NTY-bpy)]$^+$**, which is in agreement with the results obtained from luminescence imaging experiments. It has been well documented that LPS can stimulate the inflammation of macrophage cells. The above results demonstrate that the Cys level is decreased in inflammation disorders, and such a variation at subcellular levels can be monitored by both luminescence imaging and flow cytometry analysis using **[Ir(ppy)$_2$(NTY-bpy)]$^+$** as a probe.

In vivo luminescence imaging of Cys in live organisms

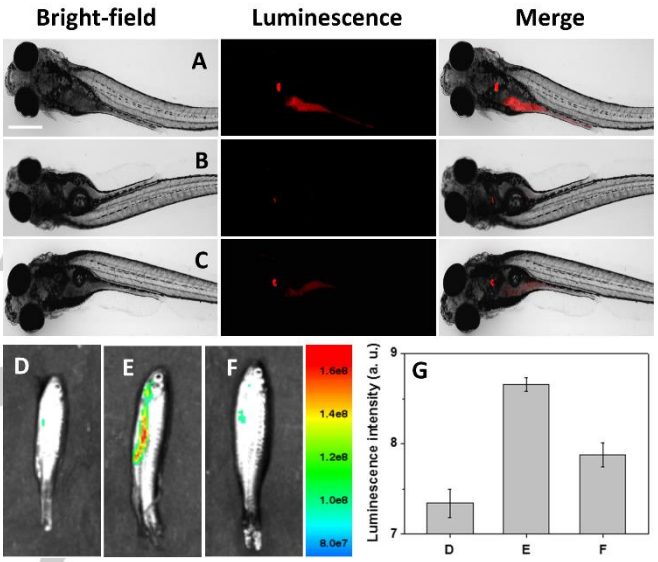

Figure 6. Bright-field, luminescence, and merged images of Cys in larval zebrafish using **[Ir(ppy)$_2$(NTY-bpy)]$^+$** as a probe. (A) Zebrafish were incubated with **[Ir(ppy)$_2$(NTY-bpy)]$^+$** (25 μM) for 1 h, (B) zebrafish were pretreated with NEM (100 μM) for 1 h, and then incubated with **[Ir(ppy)$_2$(NTY-bpy)]$^+$** (25 μM) for 1 h, (C) the group (B) zebrafish were further supplied with Cys (100 μM) for another 1 h. Scale bar, 500 μm. (D) Image of adult zebrafish; (E) zebrafish were incubated with 150 μM **[Ir(ppy)$_2$(NTY-bpy)]$^+$** for 20 min; (F) zebrafish were treated with 500 μM NEM and then incubated with 150 μM **[Ir(ppy)$_2$(NTY-bpy)]$^+$** for 20 min. Mean luminescence intensities of three groups were recorded and presented in (G).

Daphnia magna (*D. magna*) is a widely used laboratory animal as an indicator of aquatic ecosystem health and as a model animal in ecotoxicology. For evaluating the feasibility of **[Ir(ppy)$_2$(NTY-bpy)]$^+$** as a luminescent probe for imaging Cys in living organisms, *D. magna* was incubated with **[Ir(ppy)$_2$(NTY-bpy)]$^+$** (30 μM) for 1 h at 25 °C, followed by the luminescence imaging on the microscope. As shown in Figure S28A-C (Supporting Information), **[Ir(ppy)$_2$(NTY-bpy)]$^+$**-loaded *D. magna* showed strong red luminescence signals mainly in the range of the esophagus, hindgut and midgut. In a control group, a *D. magna* was pretreated with 100 μM NEM for 1 h, and then incubated with **[Ir(ppy)$_2$(NTY-bpy)]$^+$** (30 μM) for another 1 h. In this case, almost no red luminescence from *D. magna* could be observed as Cys was scavenged by NEM (Figure S28D-F, Supporting Information).

10.1002/chem.201805079

These images suggest that **[Ir(ppy)$_2$(NTY-bpy)]$^+$** could be taken up into the body of *D. magna* through feeding process, and then reacted with endogenous Cys in the digestive system to give strong red luminescence signals.

Visualization of Cys in live larval zebrafish was then performed to evaluate the *in vivo* application of **[Ir(ppy)$_2$(NTY-bpy)]$^+$**. Before imaging, the 5-day old zebrafish were pretreated with 100 μM NEM for 1 h, followed by the incubation with 25 μM **[Ir(ppy)$_2$(NTY-bpy)]$^+$** for another 1 h. For comparison, the NEM-pretreated zebrafish were further supplied with 100 μM Cys for 1 h. In a control group, the zebrafish were only incubated with 25 μM **[Ir(ppy)$_2$(NTY-bpy)]$^+$** for 1 h. The zebrafish were washed, and then subjected to the imaging. As shown in **Figure 6**, intense red luminescence signals were observed in intestine from the **[Ir(ppy)$_2$(NTY-bpy)]$^+$**-loaded fish (**Figure 6**A), while almost no luminescence was obtained for the NEM-pretreated fish (**Figure 6**B). In contrast, the red luminescence was recovered after further treating the fish with Cys (**Figure 6**C). Followed by the above imaging, the visualisation of Cys in adult zebrafish was then performed. As shown in **Figure 6**D, adult zebrafish exhibited autofluorescence slightly (**Figure 6**D), and intense luminescence signals were observed after the fish were treated with **[Ir(ppy)$_2$(NTY-bpy)]$^+$** (150 μM) for 20 min (**Figure 6**E). For the NEM-pretreated fish, the red luminescence signals almost disappeared (**Figure 6**F). All of above results demonstrate the feasibility of **[Ir(ppy)$_2$(NTY-bpy)]$^+$** for the visualisation of Cys in live zebrafish.

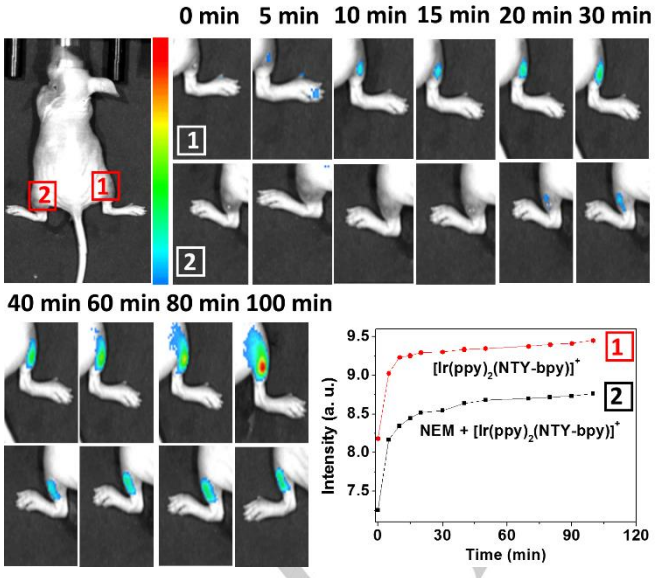

Figure 7. Luminescence imaging of Cys in live mice using **[Ir(ppy)$_2$(NTY-bpy)]$^+$** as a probe. For area 1, PBS was injected into this area for 30 min, followed by the administering of **[Ir(ppy)$_2$(NTY-bpy)]$^+$** (150 μM); for area 2, 1.0 mM NEM in PBS was injected into this area for 30 min, followed by the administering of **[Ir(ppy)$_2$(NTY-bpy)]$^+$** (150 μM). Mean luminescence intensities at each time-interval (0, 5, 10, 15, 20, 30, 40, 60, 80 and 100 min) were recorded.

The capability of **[Ir(ppy)$_2$(NTY-bpy)]$^+$** for visualization of Cys in nude mice was finally investigated. For group 1, the mice were subcutaneously injected with PBS for 30 min, followed by the administering of **[Ir(ppy)$_2$(NTY-bpy)]$^+$** (150 μM) in the same area (area 1). As the negative control, the mice in group 2 were subcutaneously injected with 1.0 mM NEM in PBS for 30 min, followed by the administering of **[Ir(ppy)$_2$(NTY-bpy)]$^+$** at the same area (area 2). Images were recorded at various time points. As shown in **Figure 7**, the luminescence signals for both **[Ir(ppy)$_2$(NTY-bpy)]$^+$** injection areas were gradually increased within 100 min, but the luminescence intensity in area 2 was clearly lower than that in area 1. These results indicate that the Cys levels in live mice can be monitored using **[Ir(ppy)$_2$(NTY-bpy)]$^+$** as a probe.

Conclusions

In conclusion, a unique Ir(III) complex, **[Ir(ppy)$_2$(NTY-bpy)](PF$_6$)**, has been designed and synthesized as a luminescent probe for sensing and imaging of Cys *in vitro* and *in vivo*. **[Ir(ppy)$_2$(NTY-bpy)]$^+$** itself exhibits weak luminescence, but shows a remarkable luminescence enhancement upon reaction with Cys. The spectrometric characterization reveals high sensitivity and selectivity of the probe in response to Cys over other amino acids. The probe shows good biocompatibility, cell-membrane permeability, and mitochondria-targeting ability, which enables the imaging and flow cytometry analysis of Cys in mitochondria of cancer cells and macrophage cells. We have also found that the Cys concentration in inflamed macrophage cells was significantly decreased, and the intracellular Cys concentration could be elevated through supplying exogenous Cys directly. These findings demonstrate the potential of the probe for the monitoring of Cys-mediated mitochondria redox activities in inflammatory disorders. Using this probe, we demonstrated luminescence sensing and imaging of Cys levels in *D. magna*, zebrafish, and live mice, which provides a new approach for the detection of Cys *in vivo*. The successful development of this probe is anticipated to contribute to the future biological researches related to the inflammation disease of live organisms.

Acknowledgements

We gratefully acknowledge the financial supports from the National Natural Science Foundation of China (Grant Nos. 21475015, 21477011, 21775015), Australian Research Council (DE170100092), National Health and Medical Research Council (APP1125794). Facilities and assistance of Queensland Node of the Australian National Fabrication Facility (ANFF-Q), the University of Queensland, are also acknowledged.

Keywords: Iridium(III) complex • Phosphorescence • Time-gated luminescence • Sensing and Imaging • Cysteine

[1] M. Garland, Joshua J. Yim, M. Bogyo, *Cell Chem. Biol.* **2016**, 23, 122.
[2] M. L. R. B. Tatiana V Mishanina, *Nat. Chem. Biol.* **2015**, 11, 457.

[3] a) X. Han, X. Song, F. Yu, L. Chen, *Adv. Funct. Mater.* **2017**, 27, 1700769; b) W. Chen, H. Luo, X. Liu, J. W. Foley, X. Song, *Anal. Chem.* **2016**, 88, 3638.

[4] a) S. Zhang, C.-N. Ong, H.-M. Shen, *Cancer Lett.* **2004**, 208, 143; b) S. S. Iyer, C. J. Accardi, T. R. Ziegler, R. A. Blanco, J. D. Ritzenthaler, M. Rojas, J. Roman, D. P. Jones, *PLOS ONE* **2009**, 4, e5017.

[5] Y. Zhang, X. Shao, Y. Wang, F. Pan, R. Kang, F. Peng, Z. Huang, W. Zhang, W. Zhao, *Chem. Commun.* **2015**, 51, 4245.

[6] D. Gong, S.-C. Han, A. Iqbal, J. Qian, T. Cao, W. Liu, W. Liu, W. Qin, H. Guo, *Anal. Chem.* **2017**, 89, 13112.

[7] K. M. H. a. T. Finkel, *Nat. Rev. Mol. Cell Biol.* **2014**, 15, 411.

[8] a) T. H. T. Candice E Paulsen, Francisco J Garcia, Arne Homann, Vinayak Gupta, Stephen E Leonard & Kate S Carroll, *Nat. Chem. Biol.* **2012**, 8, 57; b) D. W. Bak, E. Weerapana, *Mol. BioSyst.* **2015**, 11, 678.

[9] a) D. W. Bak, M. D. Pizzagalli, E. Weerapana, *ACS Chem. Biol.* **2017**, 12, 947; b) R. J. Mailloux, X. Jin, W. G. Willmore, *Red. Biol.* **2014**, 2, 123.

[10] a) B. Seiwert, U. Karst, *Anal. Chem.* **2007**, 79, 7131; b) M. J. MacCoss, N. K. Fukagawa, D. E. Matthews, *Anal. Chem.* **1999**, 71, 4527; c) T. Inoue, J. R. Kirchhoff, *Anal. Chem.* **2002**, 74, 1349; d) J. Vacek, B. Klejdus, J. Petrlova, L. Lojkova, V. Kuban, *Analyst* **2006**, 131, 1167; e) N. Shao, Y. Jin Jian, M. Cheung Sin, H. Yang Rong, H. Chan Wing, T. Mo, *Angew. Chem. Int. Ed.* **2006**, 45, 4944.

[11] a) X. Chen, F. Wang, J. Y. Hyun, T. Wei, J. Qiang, X. Ren, I. Shin, J. Yoon, *Chem. Soc. Rev.* **2016**, 45, 2976; b) R. Zhang, B. Song, J. Yuan, *TrAC Trend. Anal. Chem.* **2018**, 99, 1; c) J. A. Thomas, *Chem. Soci. Rev.* **2015**, 44, 4494; d) S. Zhen, S. Wang, S. Li, W. Luo, M. Gao, L. G. Ng, C. C. Goh, A. Qin, Z. Zhao, B. Liu, B. Z. Tang, Adv. Funct. Mater. **2018**, 28, 1706945; e) Y. Xie, Y. Xiangyu, N. Wang, Z. Yan, Y. Liu, K. Zhu, N. S. Hatzakis, X. Jiang, Adv. Funct. Mater. **2018**, 28, 1702026.

[12] H. Li, J. Fan, J. Wang, M. Tian, J. Du, S. Sun, P. Sun, X. Peng, *Chem. Commun.* **2009**, 0, 5904.

[13] a) K.-S. Lee, T.-K. Kim, J. H. Lee, H.-J. Kim, J.-I. Hong, *Chem. Commun.* **2008**, 0, 6173; b) Y. Kim, S. V. Mulay, M. Choi, S. B. Yu, S. Jon, D. G. Churchill, *Chem. Sci.* **2015**, 6, 5435.

[14] a) M. H. Lee, J. H. Han, P.-S. Kwon, S. Bhuniya, J. Y. Kim, J. L. Sessler, C. Kang, J. S. Kim, *J. Am. Chem. Soc.* **2012**, 134, 1316; b) M. Cao, H. Chen, D. Chen, Z. Xu, S. H. Liu, X. Chen, J. Yin, *Chem. Commun.* **2016**, 52, 721.

[15] a) J.-J. Shie, Y.-C. Liu, Y.-M. Lee, C. Lim, J.-M. Fang, C.-H. Wong, *J. Am. Chem. Soc.* **2014**, 136, 9953; b) F. Wang, L. Zhou, C. Zhao, R. Wang, Q. Fei, S. Luo, Z. Guo, H. Tian, W.-H. Zhu, *Chem. Sci.* **2015**, 6, 2584; c) Y. Liu, X. Lv, M. Hou, Y. Shi, W. Guo, *Anal. Chem.* **2015**, 87, 11475; d) M.-Y. Jia, L.-Y. Niu, Y. Zhang, Q.-Z. Yang, C.-H. Tung, Y.-F. Guan, L. Feng, *ACS Appl. Mater. Interfaces* **2015**, 7, 5907.

[16] a) H. M. P. H. M. M. U. K. K. K. S. N. Itoh, *Angew. Chem., Int. Ed.* **2005**, 19, 2922; b) S. Resa, A. Orte, D. Miguel, J. M. Paredes, V. Puente - Muñoz, R. Salto, M. D. Giron, M. J. Ruedas - Rama, J. M. Cuerva, J. M. Alvarez - Pez, L. Crovetto, *Chem. Eur. J.* **2015**, 21, 14772.

[17] R. Zhang, X. Yu, Z. Ye, G. Wang, W. Zhang, J. Yuan, *Inorg. Chem.* **2010**, 49, 7898.

[18] a) H. Xu, M. Hepel, *Anal. Chem.* **2011**, 83, 813; b) Y. Qi, Y. Huang, B. Li, F. Zeng, S. Wu, *Anal. Chem.* **2018**, 90, 1014.

[19] H. M. P. H. M. M. U. K. K. K. S. N. Itoh, *Angew. Chem., Int. Ed.* **2005**, 44, 2922.

[20] a) B. Tang, Y. Xing, P. Li, N. Zhang, F. Yu, G. Yang, *J. Am. Chem. Soc.* **2007**, 129, 11666; b) J. H. Lee, C. S. Lim, Y. S. Tian, J. H. Han, B. R. Cho, *J. Am. Chem. Soc.* **2010**, 132, 1216.

[21] a) R. Lincoln, L. E. Greene, W. Zhang, S. Louisia, G. Cosa, *J. Am. Chem. Soc.* **2017**, 139, 16273; b) H. S. Jung, J. H. Han, T. Pradhan, S. Kim, S. W. Lee, J. L. Sessler, T. W. Kim, C. Kang, J. S. Kim, *Biomaterials* **2012**, 33, 945.

[22] a) J. Ru, X. Chen, L. Guan, X. Tang, C. Wang, Y. Meng, G. Zhang, W. Liu, *Anal. Chem.* **2015**, 87, 3255; b) D. D. L. M. H. Z. H. K. H. L. D. S. H. C. D. C. H. Leung, *Angew. Chem. Int. Ed.* **2013**, 52, 7666; c) J. Liu, Y. Chen, G. Li, P. Zhang, C. Jin, L. Zeng, L. Ji, H. Chao, *Biomaterials* **2015**, 56, 140; d) Y. Chen, L. Qiao, L. Ji, H. Chao, *Biomaterials* **2014**, 35, 2; e) M. Wang, W. Wang, T.-S. Kang, C.-H. Leung, D.-L. Ma, *Anal. Chem.* **2016**, 88, 981; f) J. del Mármol, O. Filevich, R. Etchenique, *Anal. Chem.* **2010**, 82, 6259; g) Z. Du, B. Song, W. Zhang, C. Duan, Y.-L. Wang, C. Liu, R. Zhang, J. Yuan, *Angew. Chem. Int. Ed.* **2018**, 57, 3999; h) F. E. Poynton, S. A. Bright, S. Blasco, D. C. Williams, J. M. Kelly, T. Gunnlaugsson, *Chem. Soc. Rev.* **2017**, 46, 7706; i) L. Cao, R. Zhang, W. Zhang, Z. Du, C. Liu, Z. Ye, B. Song, J. Yuan, *Biomaterials* **2015**, 68, 21.

[23] a) H. Shi, H. Sun, H. Yang, S. Liu, G. Jekins, W. Feng, F. Li, Q. Zhao, B. Liu, W. Huang, *Adv. Funct. Mater.* **2013**, 23, 3268; b) S. Lin, W. Wang, C. Hu, G. Yang, C.-N. Ko, K. Ren, C.-H. Leung, D.-L. Ma, *J. Mater. Chem. B* **2017**, 5, 479; c) L. Tao, S. Lili, W. Erkang, D. Shaojun, *Chem. Eur. J.* **2009**, 15, 1036; d) K. Vellaisamy, G. Li, C.-N. Ko, H.-J. Zhong, S. Fatima, H.-Y. Kwan, C.-Y. Wong, W.-J. Kwong, W. Tan, C.-H. Leung, D.-L. Ma, *Chem. Sci.* **2018**, 9, 1119.

[24] a) C. Caporale, M. Massi, *Coord. Chem. Rev.* **2018**, 363, 71; b) A. M.-H. Yip, K. K.-W. Lo, *Coord. Chem. Rev.* **2018**, 361, 138; c) Z. Liu, W. He, Z. Guo, *Chem. Soc. Rev.* **2013**, 42, 1568; d) M. P. Coogan, V. Fernandez-Moreira, *Chem. Commun.* **2014**, 50, 384; e) M. R. Gill, J. Garcia-Lara, S. J. Foster, C. Smythe, G. Battaglia, J. A. Thomas, *Nat. Chem.* **2009**, 1, 662; f) K. Saeed Hiwa, J. Jarman Paul, S. Archer, S. Sreedharan, Q. Saeed Ibrahim, K. McKenzie Luke, A. Weinstein Julia, J. Buurma Niklaas, G. W. Smythe Carl, A. Thomas Jim, *Angew. Chem., Int. Ed.* **2017**, 56, 12628.

[25] F. Zhang, X. Liang, W. Zhang, Y.-L. Wang, H. Wang, Y. H. Mohammed, B. Song, R. Zhang, J. Yuan, *Biosens. Bioelectron.* **2017**, 87, 1005.

[26] W. Zhang, F. Zhang, Y.-L. Wang, B. Song, R. Zhang, J. Yuan, *Inorg. Chem.* **2017**, 56, 1309.

[27] Z.-Z. Dong, L. Lu, W. Wang, G. Li, T.-S. Kang, Q. Han, C.-H. Leung, D.-L. Ma, *Sens. Actuators B: Chem.* **2017**, 246, 826.

[28] Q. Gao, W. Zhang, B. Song, R. Zhang, W. Guo, J. Yuan, *Anal. Chem.* **2017**, 89, 4517.

[29] a) Q. Zhao, F. Li, C. Huang, *Chem. Soc. Rev.* **2010**, 39, 3007; b) C. Li, M. Yu, Y. Sun, Y. Wu, C. Huang, F. Li, *J. Am. Chem. Soc.* **2011**, 133, 11231.

[30] a) M. Zhang, Y. Wu, S. Zhang, H. Zhu, Q. Wu, L. Jiao, E. Hao, *Chem. Commun.* **2012**, 48, 8925; b) Y.-Q. Sun, M. Chen, J. Liu, X. Lv, J.-f. Li, W. Guo, *Chem. Commun.* **2011**, 47, 11029.

[31] R. E. Benesch, R. Benesch, *J. Am. Chem. Soc.* **1955**, 77, 5877.

[32] K. Qiu, Y. Chen, T. W. Rees, L. Ji, H. Chao, *Coord. Chem. Rev.* **2019**, 378, 66.

10.1002/chem.201805079

WILEY-VCH

FULL PAPER

Activatable probe specific for Cys detection in mitochondria of inflamed live cells and organisms is developed based on a unique Ir(III) complex. The probe, **[Ir(ppy)$_2$(NTY-bpy)]$^+$** is capable of phosphorescence/time-gated luminescence analysis of Cys in buffer, human sera, and live cells. Visualisation of Cys-mediated redox activities in mitochondria of inflamed cells and Cys in *D. magna*, zebrafish, and mice are demonstrated.

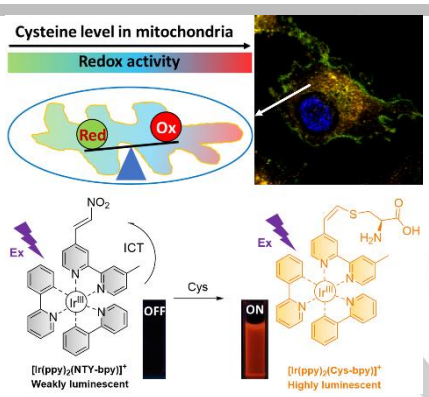

Zhongbo Du, Run Zhang, Bo Song, Wenzhu Zhang,* Yong-Lei Wang, Jianping Liu, Chaolong Liu, Zhi Ping Xu, and Jingli Yuan**

Page No. – Page No.

Iridium(III) Complex-based Activatable Probe for Phosphorescent/Time-gated Luminescent Sensing and Imaging of Cysteine in Mitochondria of Live Cells and Animals